Mon. Not. R. Astron. Soc. **000**, 1–8 (2010) Printed 1 September 2014 (MN LATEX style file v2.2)

# Dynamical evolution of V-type photometric candidates in the outer Main-belt

M.E. Huaman[1⋆], V. Carruba[1], R. C. Domingos[2]
[1] *UNESP, Univ. Estadual Paulista, Grupo de dinâmica Orbital e Planetologia, Guaratinguetá, SP, 12516-410, Brazil*
[2] *UNESP, Univ. Estadual Paulista, São João da Boa Vista, SP, 13874-149, Brazil*

arXiv:1408.7080v1 [astro-ph.EP] 29 Aug 2014

Accepted ... . Received ... ; in original form 2014 May 23

**ABSTRACT**

V-type asteroids, characterized by two absorption bands at 1.0 and 2.0 $\mu m$, are usually thought to be portions of the crust of differentiated or partially differentiated bodies. Most V-type asteroids are found in the inner main belt and are thought to be current or past members of the Vesta dynamical family. Recently, several V-type photometric candidates have been identified in the central and outer main belt.

While the dynamical evolution of V-type photometric candidates in the central main belt has been recently investigated, less attention has been given to the orbital evolution of basaltic material in the outer main belt as a whole. Here we identify known and new V-type photometric candidates in this region, and study their orbital evolution under the effect of gravitational and non-gravitational forces. A scenario in which a minimum of three local sources, possibly associated with the parent bodies of (349) Dembowska, (221) Eos, and (1459) Magnya, could in principle explain the current orbital distribution of V-type photometric candidates in the region.

**Key words:** Minor planets, asteroids: general – Celestial mechanics.

## 1 INTRODUCTION

Basaltic asteroids are associated with the crust of differentiated body. They are usually associated with a V-type spectrum, characterized by absorptions bands at 1 and 2 $\mu$ m. The majority of basaltic asteroids are found in the inner main belt, although a few have also been observed in the outer main belt. The first evidence for another possible source of basaltic asteroid in the outer main belt was the asteroid (1459) Magnya discovery by Lazarro et al. (2000). Other autors as Michtchenko et al. (2002) suggested that Magnya is a fragment from a differentiated parent body that broke up in the outer belt.

The discovery and analysis of basaltic asteroids independent of Vesta can provide insights into the early history of solar system formation (Carruba et al. **2014b, paper I hereafter**). Since the number of originally differentiated bodies that were scattered into the central and outer main belt is not well understood or constrained by previous models, and could go from a few (essentially fragments resulting from cratering events prior to the formation of the Veneneia crater on Vesta, Milani et al. **2014**), to several dozens (formation and scattering of differentiated bodies other than Vesta into the central and outer main belt, Bottke et al. 2006), setting dynamical constraints on the minimum number of independent sources of basaltic material can significantly improve our understanding of this phase of formation of our Solar System, and is one of the main goals of this paper.

This work, that is the continuation of an analogous study performed in the central main belt (**paper I), is divided as follows**: in Section 2 we revise spectral taxonomy of asteroids in the outer main belt and identify possible V-type photometric candidates. In Section 3 we define groups of V-type candidates and their possible origin. In Section 4 we obtain dynamical map of the region of the outer main belt. Section 5 is dedicated to the Yarkovsky orbital evolution, with a subsection on the long-term effect of close encounter with massive asteroids. Finally, we present our conclusions in Section 6.

## 2 IDENTIFICATION: SPECTRAL TAXONOMY AND SDSS-MOC4 DATA

In this section we use the classification method used in **paper I**, and based on the work of DeMeo and Carry (2013). This method employs SDSS-MOC4 gri slope and $z' - i'$ colors to classify an asteroid depending its position on that plane.

⋆ E-mail: mariela@feg.unesp.br

As a first part of our analysis, we checked if the preliminary study of the taxonomy of the candidate V-type asteroids obtained in **paper I** still holds. We identified 14 possible V-type candidates in the outer main belt, 5 of which were spectroscopically observed and classified as V-types (1459 Magnya, Lazzaro et al. (2000), 7472 Kumakiri, Duffard and Roig (2009), 10537 1991 RY16 Moskovitz et al. (2008), 14390 1990 QP19, De Sanctis (2011a,b), 105041 2000 K041, De Sanctis et al. (2011a,b)). Six objects (11465, 55270, 91159, 92182, 177904, and 208324) were reported in Table 1 of **paper I**, while one (34698 2001 OD22, also listed in the WISE albedo catalog[1]) is a newly identified V-type photometric candidate.

V-type asteroid candidate were identified in the past by Carvano et al. (2010). These authors used studies on taxonomy of asteroids observed by the Sloan Digital Sky Survey-Moving Object Catalog data, fourth (SDSS-MOC4 hereafter), and identified 52 V-type photometric candidates in the outer main belt, including objects with QS, SV, and other cases. This database is available on the Planetary Data System (http:sbn.psi.edu/pds/resource/sdsstax.html, and was accessed on November $16^{th}$ 2013).

With respect to this database, we selected all asteroids that were V-type photometric candidates (including object with QS, SV and other cases) and identified according to the HORIZONS System of the Jet Propulsion Laboratory (Giorgini et al. 1996). Except the five confirmed V-type asteroids, we encountered 25 V-type candidates that are pure V (excluding QS and SV cases) and have proper elements as reported by the AstDyS site. Also considering the seven new candidates identified in this work and in **paper I**, and the five confimed V-type objects, we have a total of 37 asteroids that are possible or confirmed V-types in the outer main belt (with known proper elements).

Fig. 1 displays a proper $(a, e)$ (panel A), and $(a, sin(i))$ (panel B) projections of the proper elements of all candidates (black dots), the pure V-type candidates (green full dots) and of the confirmed V-types asteroids (red full dots). Vertical lines represent the location of the main local mean-motion resonances, blue lines show the positions of the center of secular resonances, computed using the analytical theory of Milani and Knežević (1994) to determine the proper frequencies $g$ and $s$ for the grid of $(a, e)$ and $(a, \sin(i))$ values shown in Fig. 1 and the values of angles and eccentricity of (31) Euphrosyne, the asteroid with the largest family in the highly inclined region.

We can observe in Fig. 1 three regions of concentrations of V-types candidates in the $(a, sin(i))$ plane. One region is around Magnya (Magnya region hereafter) and is between the resonances 7J:-3A and 2J:-1A. This region includes the confirmed V-type asteroid (1459) Magnya, with a range values of $sin(i)$ of $0.24 < sin(i) < 0.40$ . A higher concentration near the Eos family is found in the center of the outer main belt (Eos region, since Eos has been suggested as a possible source of basaltic material in the past, Mothé-Diniz et al. 2008) between the resonances 7J:-3A and 2J:-1A, with $0.00 < sin(i) < 0.24$. Finally, in the region between the resonances 5J:-2A and 7J:-3A and $sin(i) < 0.40$, we found some scattered objects that may have passed through the resonance 5J:-2A. Since Moskovitz et al. (2008) suggested that (349) Dembowska could be a parent body of a differentiated family, and because of the presence of the Koronis family in the region, another possible source of differentiated objects, we define this area as the Koronis and Dembowska region.

Four V-type photometric candidates were members of asteroid families, two in the Koronis and two in the Eos families, respectively. Following the approach of **paper I**, we estimated the probability that such occurrences were produced by a Poisson distribution. Considering a standard Poisson distribution (see also **paper I**, Eq. 1), the probability that a number of objects be produced by a Poisson distribution assuming that the expected number of k occurrence in a given interval is given by Eq. 1 in **paper I**. For our purposes we used for the expected number of occurrences in the given interval the mean values of objects expected in the regions of the Koronis and Eos families, given by Eq. 2 in **paper I**.

We used simple **parallelepipedal** regions for the areas occupied by the Koronis and Eos families, defined according to the minimum and maximum values in $(a, e, sin(i))$ observed for the halos of these two families in Carruba et al. (**2013**), defined as $2.828 < a < 2.987\ au, 0.0112 < e < 0.082, 0.0128 < sin(i) < 0.058$, and $2.915 < a < 3.186\ au, 0.036 < e < 0.108, 0.144 < sin(i) < 0.207$, respectively. $v_{Tot}$, the total volume occupied by all photometric candidates, was defined as the region between the 5J:-2A and 2J:-1A mean motion resonances with Jupiter in semi-major axis (i.e., $2.8258 < a < 3.279\ au$), and eccentricity and $sin(i)$ from zero to the maximum value of any V-type candidate in the outer main belt, i.e., 0.2738 and 0.4. Using Eq. 1 in **paper I**, we found that the probability that the two asteroids in the Koronis family region, and the six in the Eos **parallelepipedal** region (four of these objects are not members of the Eos dynamical family) could be explained as fluctuations of a Poissonian distribution are of $4.53 \times 10^2$, and $2.53 \times 10^4$. Considering that the null hypothesis threshold is equal to $1.0 \times 10^2$), while the results for the Koronis region may possibly be compatible with fluctuations of a Poissonian distribution, those for the Eos region seem more robust and may indicate a possible local source.

Since 1-dimensional statistical analysis are somewhat dependent on the choice of the regions boundaries, and following the approach of **paper I**, we also perfomed **Mardia's** test (Mardia 1970) on multivariate normality for the whole 35 V-type photometric candidates population. Values of the $A$ and $B$ parameters described in **paper I** were incompatible with $\chi^2$ and a normal distribution, which excludes that V-type photometric candidates follow a tri-variate Gaussian distribution as a whole. In the next section we will further analyze the three orbital regions defined in this section.

[1] Initial results from the Wide-field Infrared Survey Explorer (WISE) (Wright et al. 2010), and the NEOWISE (Mainzer et al. 2011) enhancement to the WISE mission recently allowed to obtain diameters and geometric albedo values for more than 100,000 Main Belt asteroids (Masiero et al. 2011).

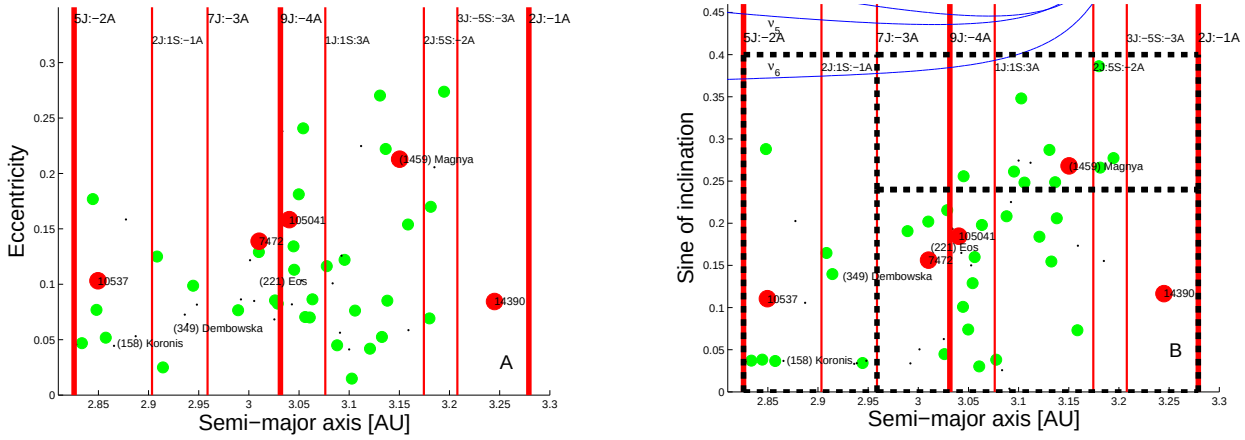


**Figure 1.** Panel A: Proper semi-major axis versus eccentricity of the V-type candidates identified using SDSS-MOC4 data in the outer main belt. Panel B: Semi-major axis versus sine of proper incliation of the V-type candidates. Vertical lines displays mean-motion resonances, blue lines show the location of secular resonances, black dotted lines the limits of the regions in the $(a, sin(i))$ plane. See text for a discussion of the other symbols.

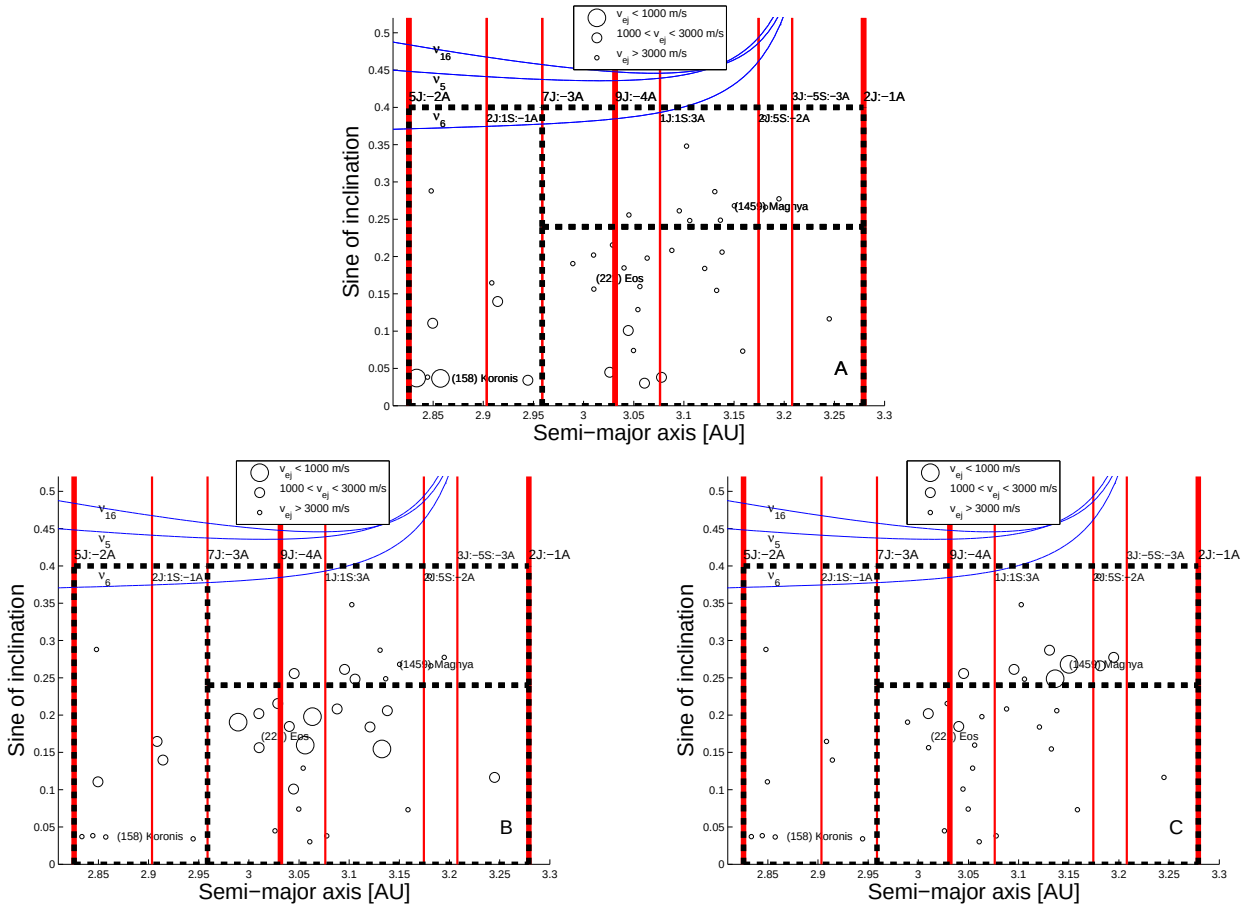


**Figure 2.** An $(a, sin(i))$ projection of V-type photometric candidates in the outer main belt. Distances with respect to the asteroids (158) Koronis (panel A), (221) Eos (panel B), and (1459) Magnya (panel C) are shown with the **symbol syze code** discussed in the text.

## 3 GROUPS OF V-TYPE CANDIDATES AND THEIR POSSIBLE ORIGIN

To further investigate the robustness of the three regions introduced in Sec. 2, we computed the distances of all photometric V-type candidates in the outer main belt with respect to the three suggested possible parent bodies: (158) Koronis and (349) Dembowska, (221) Eos, and (1459) Magnya. To determine the distances we used the standard metrics of Zappalá et al. (1995) (see also Eq. 7 in **paper I**).

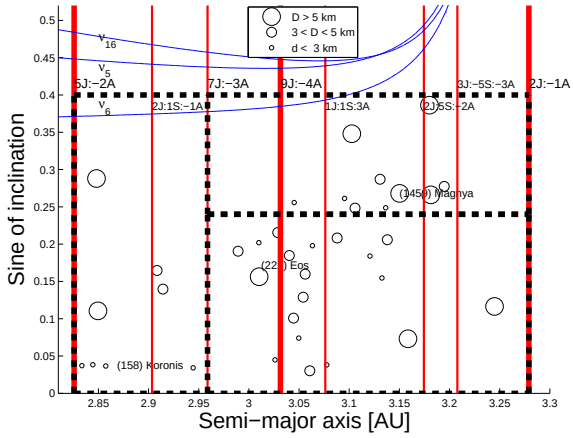


**Figure 3.** An $(a, sin(i))$ projection of V-type photometric candidates in the outer main belt. The size **of the symbols** is associated with the asteroid diameter, according to the figure legend.

Results are shown in the three panels of Fig. 2. Asteroids with distances $d$ with respect to (158) Koronis (panel A), (221) Eos (panel B), and (1459) Magnya (panel C) less than 1000 m/s are rendered as **large black open circles**, those with $1000 < d < 3000$ m/s are shown as **medium-size black circles**, and **small circles** identify the objects with $d > 3000$ m/s. The other symbols are the same as in Fig. 1.

Overall, except for a few outliers and two highly inclined objects (11465 and 34698) in the Magnya region, the closest objects to each of the three possible parent bodies tend to be found in its own region, suggesting that the regions that we proposed in the previous section might be a robust feature.

How much mass is contained in the V-type photometric candidates in the outer main belt? To answer this question, we considered the V-type candidates with diameter values from the WISE mission (12 objects) and for the others we computed their diameter using the relationship of Harris and **Lagerros** (2002) (see also Eq. 8 in **paper I**). The minimum and maximum values of the albedo $p_V$ were 0.040 and 0.392, respectively. Our results are shown in Fig. 3, where larger asteroids with $D > 5$ km are shown as **large black open circle, medium-size black circles show the position of the asteroids with** $3 < D < 5$ **km, and the small circles** are associated with smaller bodies.

To estimate how much mass in the currently known V-type candidates is present in the outer main belt, we used the equation 9 from **paper I** (Moskovitz et al. 2008), where the bulk density was assumed equal to 3000 kg/m$^3$, value typical of V-type objects. For our candidates, we obtained a total mass of $1.75 \times 10^{16}$ kg, which is 1.35% of the estimated mass escavated from craters in Vesta $1.3 \times 10^{18}$ kg; more than the 0.139% found by **paper I** for the total mass of V-type candidates in the central main belt, but still a very small fraction of the observed basaltic material in the inner main belt. In the next section we will discuss how V-type photometric candidates interact with the local web of mean-motion and secular resonances.

## 4 DYNAMICAL MAPS

We continue our analysis by studying the orbital region of V-type photometric candidates in the outer main belt. We obtained a dynamical map of synthetic proper elements with 18391 test particles using the integrational set-up described in **paper I**. We used a step in $a$ of 0.003 **au** and in $i$ of 0.2° and took particles in an equally spaced grid of 152 by 121 in the $(a, sin(i))$ plane, the representative plane for studying diffusion of members of asteroid families[2]. The initial values of $e, \Omega, \omega$, and $\lambda$ of the test particles were fixed at those of (221) Eos, the largest member of its family and a possible source of V-type asteroids. We then computed synthetic proper elements $(a, e, sin(i))$ and frequencies $(n, g, s)$ of these test particles with the approach described in Carruba (2010).

Fig. 4 displays a projection in the $(a, sin(i))$ plane of the results of our simulations. Black dots are associated with the orbital position of each simulated particle. Mean-motion resonances appear as vertical bands with lesser density of test particles [3], secular resonances show as inclined alignments of test particles. Other symbols in the figure have the same meaning as in Fig. 1, panel B. The main secular resonance in the outer main belt to appear in our map is the $z_1 = g - g_6 + s - s_6$ secular resonance. We selected test particles whose combination of asteroidal secular frequencies are to within 0.5 arcsec/yr with respect to the resonance center (i.e., g+s = $g_6 + s_6$): these particles are identified by blue circles in Fig. 1. Other secular resonances are present in the outer main belt but plays a lesser role when the Yarkovsky force is considered: except for the $z_1$ and $2\nu_5 - 2\nu_6 + \nu_{16}$ resonances, Carruba et al. (2014a) showed that the fraction of objects in librating states of other resonances drops to less than 40% of the original population after 100 Myr.

Nevertheless, we studied the time dependence of the resonant argument of resonances that showed to be dynamically important in Carruba et al. (2014a) for the whole 37 V-type photometric candidates populations that we identified in Sect. 2. In particular, we observed the time-dependence of the resonant angles of the resonances $z_1, z_2, z_3, 2\nu_5 - 2\nu_6 + \nu_{16}, 3\nu_6 - 2\nu_5, 2\nu_6 - \nu_5$, and $\nu_5 + \nu_{16}$. With respect to the central main belt, where **paper I** identified a population of 28 V-type photometric candidates in secular resonant states, 15 of which inside the $2\nu_6 - \nu_5$ resonance, in the outer main belt we only found one object (85812 1998 WR22) inside the $3\nu_6 - 2\nu_5$ resonance. Three objects were in circulating orbits close to the separatrix of the $z_1$ resonances, and three other asteroids were also near the separatrix of the $2\nu_5 - 2\nu_6 + \nu_{16}$ resonance. While past interactions with secular resonances may of course not be excluded, overall secular dynamics seems to have played a lesser role in the dynamical evolution of V-type photometric candidates in the central main belt with respect to the outer belt. Further assessing the truth of this statement will be one of the subjects of the next section.

[2] Our particles covered a range between 2.825 and 3.278 **au** in $a$, and 0° and 24.0° in $i$, respectively.

[3] Of particular interest is the confirmed V-type asteroid 14390 (1990 QP19), that is on the edge of the stable region near the 2J:-1A mean-motion resonance separatrix.

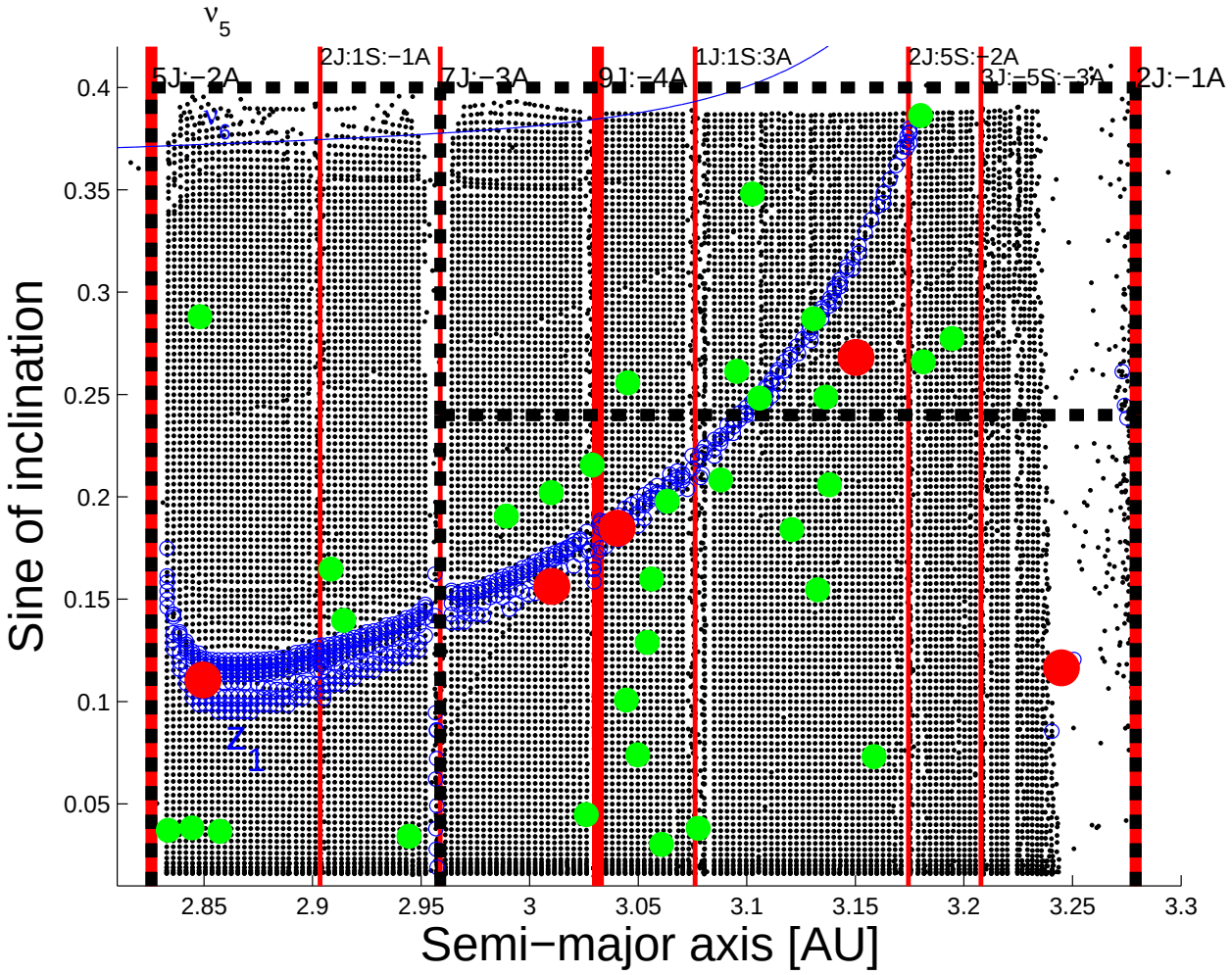


**Figure 4.** An $(a, sin(i))$ proper element map of the outer main belt. Black dots identify the orbital position in the plane of proper $(a, sin(i))$ of each simulated test particle. **Blue open** circles are associated with asteroids likely to be in $z_1$ secular resonance configurations. The other symbols have the same meaning as in Fig. 1.

## 5 DYNAMICAL EVOLUTION

To investigate the dynamical evolution of the 37 V-type candidates in the outer main belt, we used the same methods and procedures presented in (**paper I**. We integrated clones of these objects with SWIFT-RMVSY, the symplectic integrator of Brož (1999). As in **paper I**, we used the two sets of spin axis orientations with $\pm 90^\circ$ with respect to the orbital plane that maximize the velocity of the drift caused by the Yarkovsky effect, and did not considered re-orientations. To further investigate the dynamical evolution of V-type candidates in the outer main belt, we performed 'fast' and 'slow' numerical simulations of these asteroids, assuming that all asteroids had 100 m diameters, and then using the real diameters. Our results are presented in Figs. 5 and 6, which refer to the final orbital evolution on the $(a - sin(i))$ plane of V-type photometric candidates in the region of Eos, Koronis and Magnya.

### 5.1 Results of the fast simulations

We obtained synthetic proper elements every 1.2 Myr for all the simulated asteroids, with the approach used in **paper I**, over 200 Myr. In Fig. 5 we show the dynamical paths of clones of particles in the Dembowska region (panel A), Eos (panel B) and Magnya (panel C) in the $(a, sin(i))$ plane. Blue dots represent snaphsots of the orbital evolution of clones of real asteroids with $0^\circ$ obliquity, while yellow dots are associated with clones with $180^\circ$ obliquity.

In the Koronis region there were eight photometric candidates. Four of them were not able to cross the 7J:-3A mean-motion resonance, including the (10537) V-type confirmed body. This could suggest that communication between the Koronis and Eos region is in principle possible, even if on long time-scales. In panel B we observe the orbital evolution of 19 asteroids in the Eos region: only 3 of them were not able to cross the 7J:-3A mean-motion resonance, and all clones were able to cross the 9J:-4A and 3J:-5S:-3A mean-motion resonances, until reaching the powerful 2J:-1A mean-motion resonance. Panel C deals with the or-

bital evolution of the 10 photometric candidates in the Magnya region. Three objects were not able to cross the 9J:-4A mean-motion resonance, and only one managed to pass the 7J:-3A resonance. No asteroids crossed the 2J:-1A mean-motion resonance and the $\nu_6$ secular resonance. Overall, we found one particle that managed to cross the main dynamical barrier of the 5J:-2A resonance and none that crossed the 2J:-1A mean motion resonance, suggesting that comunication between the central and outer main belt might be possible, but not likely (how effective is this mechanism for larger asteroids will also be discussed in Sect 5.2.

Finally, we also observed minor changes of inclination caused by secular resonances (mostly by the $z_1$ resonance) for some particles, but not enough to allow them to change region. Based on the results of these "fast simulations" we may conclude that communication between the Koronis and Eos regions and between the Koronis and Magnya regions may be possible, but that passing from the Eos to the Magnya region and vice-versa might a more unlikely event. We will further investigate this hypothesis in the next subsection.

### 5.2 Results of the slow simulations

To further investigate the dynamical evolution of V-type candidates in the outer main belt, we also performed slow simulations of clones of the same particles studied in Sect 5.1. We took the WISE values of the diameters for the test particles for which such information was available, and we used the methods described in Sect 3 for the other particles. We also took six values of spin obliquities, 0° , 30° , 60° , 120° , 150° , and 180°, in order to sample different speeds of drifts caused by the Yarkovsky force. We integrated our test particles over 1 Byr, with the same integration scheme used in Sect 5.1. As in **paper I**, because of the longer integration time used in these runs, we computed proper elements every 4.9 Myr instead of the 1.2 Myr used in Sect 5.1.

Fig. 6 displays the time evolution of proper $(a, sin(i))$ values for clones of V-type photometric candidates with obliquities of 60° and 150° in the Koronis region, with **obliquities** of 0° and 180° in the Eos region, and with obliquities of 60° and 150° in the Magnya region (panels A, B, and C, respectively). Prograde **rotation** clones elements are shown as blue dots, retrograde **rotation** clones ones are identified as yellow dots. Other symbols are the same as those used in Fig. 5. Results are similar for other values of the obliquities, and will not be shown for the sake of brevity.

Of the 222 integrated clones, none was able to go from the Koronis region to the Eos and Magnya areas or to cross the 7J:-3A mean-motion resonance. Only 2 particles from the Eos region managed to cross the 7J:-3A mean-motion resonance and go into the Koronis area, i.e., 1.8% of the total, suggesting that communication across the 7J:-3A mean-motion resonance should be a relatively rare event.

More difficult to interpret were the results near the boundaries of the Magnya and Eos region. Of the 114 integrated clones in the Eos area, 3 particles (2.7%) managed to reach the Magnya area and survive (mostly because of interaction with the $z_1$ secular resonance). Conversely, of the 60 particles integrated in the Magnya region, only 5 (4.5%) were able to reach the Eos region via diffusion in the $z_1$ secular resonance and interaction with other mean-motion

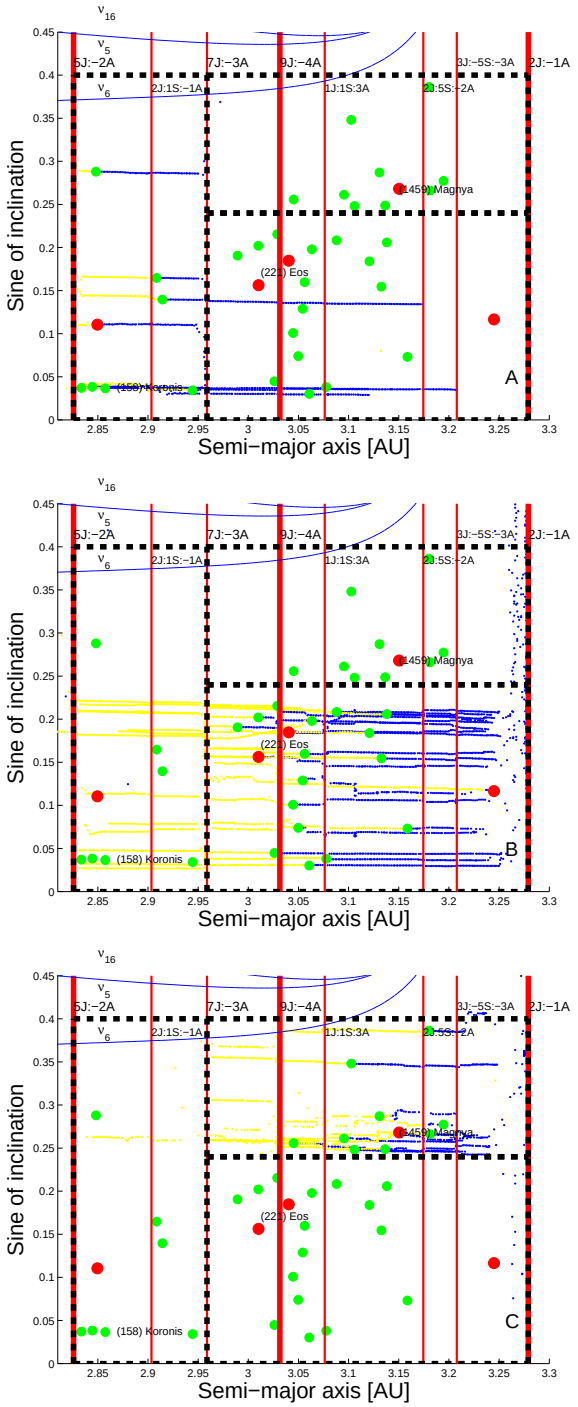


**Figure 5.** Orbital evolution of 100 m clones of V-type photometric candidates in the region of Eos, Koronis and Magnya. See text for further details on the symbols used in this figure.

resonances in the area, and remain there stably. In all the six simulations, we only observed 3 particles that managed to cross the 9J:-4A main-motion resonance and approach the 7J:-3A, resonance, but were not able to cross it. (1459) Magnya is confined in a zone defined by the $z_1$ and 2J:-1A resonances, and no particles managed to cross the $\nu_6$ **secular** resonance.

Overall, communication between the Eos and Magnya region seems possible, but not on scale large enough to dis-

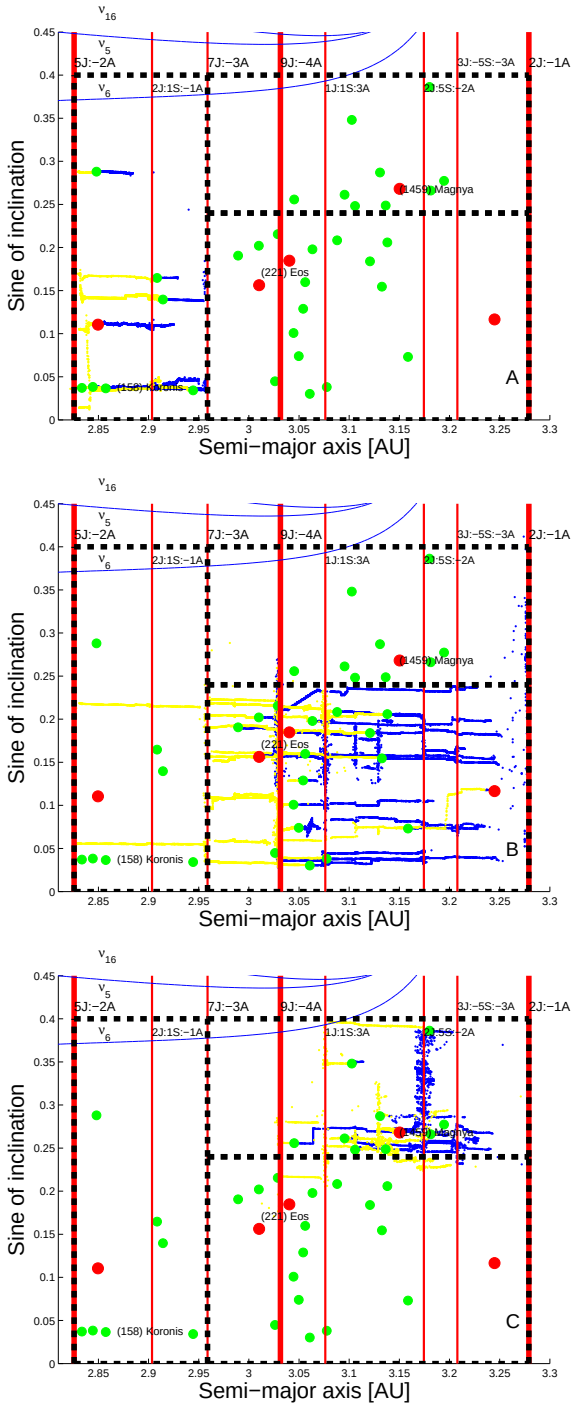


**Figure 6.** Orbital evolution of clones of real asteroids in the region of Koronis, Eos, and Magnya, integrated over 1 Byr. Other symbols are the same as those used in Fig. 5.

miss the two source scenarios for these regions. While some mixing among V-type photometric candidates coming from the Magnya and Eos parent body could be possible, our results still seems to suggest a minimum of three-sources to explain the current population of V-type photometric candidates in the outer main belt.

### 5.3 Effect of close encounter with massive asteroids

**Paper I** recently estimated the long term effect of diffusion caused by close encounters with three massive asteroids in the central main belt, including (1) Ceres, the most massive body in the main belt, and by far the most effective perturber. Under the assumption that long-term effect of close encounters can be modeled, in first approximation, as a random walk with zero mean, there will be a $1\sigma$ ($= 68.27\%$) probability that the root mean square translation distance (or quadratic mean) after $n$ steps will fall between $\pm\sigma_{sin(i)}\sqrt{n}$, where $\sigma_{sin(i)}$ is the standard deviation of changes in $\sin(i)$, equal to 0.0029 for the distribution of changes in $i$ caused by (1) Ceres over 200 Myr. For 4 Byr, the maximum time for which Bottke et al. (2006) estimated the possible arrival of differentiated bodies in the main belt, the root mean square translation in $\sin(i)$ would be of 0.0130. Considering our boundary between the inclination regions of Eos and Magnya at $\sin(i) = 0.24$, there are only 2 Magnya objects ((63075) 2000 WC126 and (188331) 2003 OZ32) that could have changed inclination region over 4 Byr only because of encounters with massive asteroids, i.e., 5.4% of the total. Overall, close encounters with massive asteroids may have furnished an additional mechanism for dynamical mobility, but alone could not have produced substantial mixing between the Eos and Magnya regions.

## 6 CONCLUSIONS

The main goal of this article was to study possible diffusion paths of V-type photometric candidates in the the outer main belt. For these purposes, we:

- Revised the current knowledge on confirmed and pure V-type photometric candidates from SDSS-MOC4 data in the area. Using the DeMeo and Carry (2013) approach, we identified 7 new V-type photometric candidates in the region for a total of 37 possible V-type asteroids in the outer main belt. Six asteroids appear to be members of the Eos family, and statistical considerations suggest that Eos could be a possible local source of basaltic material.
- Identified three regions in the $(a, sin(i))$ plane associated with three possible local sources of basaltic material: the parent bodies of (349) Dembowska, (221) Eos, and (1459) Magnya. We computed distances of the V-type photometric candidates and masses of these objects. The closest objects to each of the three possible parent bodies tend to be found in its own regions, suggesting that these regions may be robust features. Only 1.35% of the mass escavated from the craters in Vesta is currently present in the outer main belt.
- Obtained a synthetic proper element map for 18391 particles in the outer main belt. The $z_1$ secular resonance is the main non-linear secular resonance in the area, and we found only one asteroid (85812 WR22) in non-linear secular librating states, inside the $3\nu_6 - 2\nu_5$.
- Studied the dynamical evolution of clones of V-type photometric candidates in the area under the influence of Yarkovsky and YORP forces, and estimated the long-term effect of close encounters with massive asteroids. Overall, our results seems to indicate a possible three sources scenario for

the origin of basaltic material in the outer main belt, possibly associated with the parent bodies of (349) Dembowska, (221) Eos, and (1459) Magnya. While communication across the 7J:-3A mean-motion resonance seems to be a rare event, up to $\simeq 20\%$ of bodies from the Magnya region could have reached the Eos area. Mixing between the Magnya and Eos population could be possible, but not on scales large enough to rule out a three source scenario.

Overall, the main result of our analysis suggest that a minimum three sources scenario is needed to explain the current orbital distribution of V-type photometric candidates in the outer main belt. Contrary to the case of the central main belt, mixing between different zones material may occur in somewhat larger proportion (up to 5%), but communication across the 7J:-3A mean-motion resonance seems an unlikely event for km-sized asteroid. A study of mineralogical properties of V-type photometric candidates in the region could in principle provide further clues to the possible origin of basaltic material in the outer main belt, and on our three-sources scenario hypothesis.

## ACKNOWLEDGMENTS

We thank an anonymous reviewer for comments and suggestions that significantly improved the quality of this paper. We would like to thank the São Paulo State Science Foundation (FAPESP) that supported this work via the grant 11/19863-3, and the Brazilian National Research Council (CNPq, grant 305453/2011-4). This publication makes use of data products from the Wide-field Infrared Survey Explorer, which is a joint project of the University of California, Los Angeles, and the Jet Propulsion Laboratory/California Institute of Technology, funded by the National Aeronautics and Space Administration. This publication also makes use of data products from NEOWISE, which is a project of the Jet Propulsion Laboratory/California Institute of Technology, funded by the Planetary Science Division of the National Aeronautics and Space Administration.

## 7 APPENDIX

Table 1 reports the asteroid identification, its proper $a, e$, and $sin(i)$, its absolute magnitude ($H$), diameter ($D$), and geometric albedo ($p_V$), according to the WISE mission, when available, for all asteroids in the central main belt identified in Carvano et al. (2010). Asteroids without WISE data on $D$ and $p_V$ have been assigned the mean value of geometric albedo of V-type asteroids in the outer main belt, and diameters computed according to Eq. 8 in **paper I** (for simplicity, we do not report these data in the Table).

## REFERENCES

Bottke, W. F., Nesvorný, D., Grimm, R. E., Morbidelli, A., O'Brien, D. P., 2006, Nature, 439, 821.
Brož, M., 1999, Thesis, Charles Univ., Prague, Czech Republic.
Carruba, V., 2010, MNRAS, 408, 580.
Carruba, V., Domingos, R. C., Nesvorný, D., Roig, F., Souami, D., 2013, MNRAS, 437, 2279.
Carruba, V., R. C. Domingos, Huaman, M. E., Dos Santos, C. R., Souami D., 2014a, MNRAS, 437, 2279.
Carruba, V., Huaman, M. E., Domingos, R. C., Dos Santos, C. R.,Souami D., 2014b, MNRAS, 439, 3168.
Carvano, J. M., Hasselmann, P.H., Lazzaro, D., Mothé-Diniz, T., 2010, A&A, 510, A43.
DeMeo, F., Carry, B. 2013, Iracus, 266, 723.
**De** Sanctis, M. C., Ammannito, E., Migliorini, A., and **5 co-authors** 2011a, MNRAS, 412, 2318.
**De** Sanctis, M. C., Migliorini, A., Luzia Jasmim, F., and **5 co-authors** 2011b, EPSC-DPS Joint Meeting 2011, 212 .
Duffard, R., **and** Roig, F. 2009, P&SS, 57, 229.
Giorgini, J. D., and 9 co-authors, Bulletim of the American Astronomical Society 28, 1158, http://ssd.jpl.nasa.gov.ssd.jpl.nasa.gov/horizons.cgi.
Harris, A. W., Lagerros, J. S. V., 2002, Asteroids III, W. F. Bottke Jr., A. Cellino, P. Paolicchi, and R. P. Binzel (eds), University of Arizona Press, Tucson, 205-218.
Knežević, Z., Milani, A., 2003, A&A, 403, 1165.
Lazzaro, D., and 10 co-authors, 2000, Science, 288, 2033.
Mardia, K., V., 1970, Biometrika 57, 519.
Masiero, J. R., and 17 co-authors, 2011, ApJ 741, 68.
Mainzer, A. K., and 35 co-authors, 2011, ApJ 731, 53.
Machuca, J. F., Carruba, V., 2012, MNRAS, 420, 1779.
Milani, A., Knežević, Z. Icarus, 1994, 107. 219.
Milani, A., Cellino, A., Knezevic, Z., and 3 co-authors, 2014, Icarus 239, 46.
Michtchenko, T. A., Lazzaro, D., Ferraz-Mello, S., Roig, F. 2002, Icarus, 158, 343.
Moskovitz, N. A., and 4 co-authors, 2008, AJ, 682, 57.
Mothé-Diniz, T., Carvano, J. M., Bus, S. J., Duffard, R., Burbine, T. H. 2008, Icarus, 195, 277
Wright, E. L., and 38 co-authors, 2010, AJ, 140, 1868.
Zappalà, V., Bendjoya, Ph., Cellino, A., Farinella, P., Froeschlé, C., 1995, Icarus, 116, 291.

This paper has been typeset from a TEX/ LATEX file prepared by the author.

**Table 1. List of V-type photometric candidates in the outer main-belt.**

| # Asteroid id. | $a$ | $e$ | $sin(i)$ | H | D(km) | $P_v$ | Family |
|---|---|---|---|---|---|---|---|
| **(349) Dembowska - (158) Koronis** | | | | | | | |
| 10537 | 2.8496 | 0.1032 | 0.1105 | 12.41 | 7.8650 | 0.3131 | |
| 36590 | 2.8336 | 0.0468 | 0.0371 | 14.64 | 2.7020 | 0.1674 | Koronis |
| 55270 | 2.9085 | 0.1250 | 0.1647 | 14.02 | | | |
| 52726 | 2.8481 | 0.0769 | 0.2880 | 13.35 | | | |
| 55613 | 2.9143 | 0.0250 | 0.1397 | 14.34 | | | |
| 85812 | 2.8444 | 0.1769 | 0.0383 | 15.04 | | | |
| 141036 | 2.9444 | 0.0987 | 0.0342 | 15.78 | | | |
| 160435 | 2.8573 | 0.0518 | 0.0366 | 16.35 | | | Koronis |
| **(221) Eos** | | | | | | | |
| 7472 | 3.0102 | 0.1389 | 0.1563 | 12.08 | 10.0080 | 0.2795 | |
| 14390 | 3.2449 | 0.0844 | 0.1165 | 12.16 | 10.7670 | 0.2202 | |
| 41243 | 2.9893 | 0.0766 | 0.1906 | 14.36 | 4.2160 | 0.1727 | Eos |
| 58860 | 3.0561 | 0.0704 | 0.1598 | 14.28 | 3.7390 | 0.1665 | Eos |
| 61877 | 3.0607 | 0.0700 | 0.0302 | 14.75 | | | |
| 63085 | 3.1380 | 0.0852 | 0.2059 | 14.16 | | | |
| 65256 | 3.0880 | 0.0449 | 0.2083 | 14.27 | | | |
| 97502 | 3.0541 | 0.2407 | 0.1289 | 14.43 | 3.0460 | 0.2751 | |
| 105041 | 3.0403 | 0.1583 | 0.1847 | 14.09 | | | |
| 106205 | 3.0776 | 0.1163 | 0.0381 | 15.50 | | | |
| 117043 | 3.0260 | 0.0854 | 0.0448 | 15.17 | | | |
| 144548 | 3.1207 | 0.0419 | 0.1840 | 15.24 | | | |
| 153284 | 3.0445 | 0.1342 | 0.1008 | 14.83 | | | |
| 177904 | 3.1586 | 0.1539 | 0.0731 | 15.30 | 5.762 | 0.0403 | |
| 189899 | 3.0099 | 0.1291 | 0.2020 | 15.20 | | | |
| 195852 | 3.1326 | 0.0525 | 0.1546 | 15.62 | | | |
| 225034 | 3.0288 | 0.0825 | 0.2155 | 14.81 | | | |
| 261676 | 3.0497 | 0.1812 | 0.0740 | 15.67 | | | |
| 301865 | 3.0634 | 0.0864 | 0.1979 | 16.52 | | | Eos |
| **(1459) Magnya** | | | | | | | |
| 1459 | 3.1503 | 0.2129 | 0.2681 | 10.24 | 29.900 | 0.2168 | |
| 11465 | 3.1026 | 0.0149 | 0.3480 | 12.87 | 12.556 | 0.0775 | |
| 34698 | 3.1800 | 0.0692 | 0.3863 | 12.42 | 8.070 | 0.3920 | |
| 63075 | 3.1058 | 0.0762 | 0.2482 | 13.97 | 3.778 | 0.2358 | |
| 91159 | 3.1946 | 0.2738 | 0.2773 | 14.28 | | | |
| 92182 | 3.1813 | 0.1699 | 0.2660 | 13.70 | | | |
| 141050 | 3.0954 | 0.1220 | 0.2613 | 14.97 | | | |
| 188331 | 3.1364 | 0.2221 | 0.2487 | 15.21 | | | |
| 208324 | 3.1307 | 0.2703 | 0.2870 | 14.91 | | | |
| 311474 | 3.0452 | 0.1131 | 0.2557 | 15.28 | | | |